Journal of Metals, Materials and Minerals, Vol. 32, No. 3, pp. 43-53, 2022

Sm^{3+} doped Mn-Zn mixed ferrites: Synthesis and characterization

Anjali SHRIVASTAVA[1,*], and Ashwani Kumar SHRIVASTAVA[1]

[1]*School of Studies in Physics, Jiwaji University, Gwalior (M.P.) – 474011, India*

***Corresponding author e-mail:** success.anjali208@gmail.com

Received date:
17 May 2022
Revised date
13 July 2022
Accepted date:
18 July 2022

Keywords:
Ferrites;
Rare earth;
XRD;
SEM;
VSM

Abstract

Pure and Samarium (Sm^{3+}) doped Mn-Zn ferrites were synthesized using Co-precipitation method. The Sm^{3+} concentration varied from 0.1% to 0.3%. This was added to the solution during the synthesis of Mn-Zn ferrites ($Mn_{0.5}Zn_{0.5}Fe_2O_4$) at room temperature. The precipitate so obtained was annealed at 200°C for 4 h and then crushed to powder. The powdered material was subjected to structural, morphological, compositional, optical and magnetic characterization. XRD shows cubic spinal structure with crystallite size of the order of 6 nm. TEM and SEM images show spherical particles are in good agreement with XRD data. EDAX indicates stoichiometry of elements present in material. FTIR shows various functional groups and doped samarium. VSM for pure Mn:Zn ferrite show hysteresis with high magnetization, coercivity and low remanence. All the magnetic parameters decrease on 0.1% Sm^{3+} doping. These parameters get increased, compared to values at 0.1% doping, on increasing Sm^{3+} doping to 0.2%. On further increasing Sm^{3+} doping to 0.3%, the magnetic parameters show insignificant changes. VSM shows that Sm^{3+} affects magnetic properties significantly only at lower doping concentrations. These changes are due to Sm^{3+} substitution at tetrahedral and octahedral positions. The ionic radii mismatch in between Samarium and iron influence the magnetic parameters of $Mn_{0.5}Zn_{0.5}Fe_2O_4$.

1. Introduction

Mn-Zn ferrites (MZF) belong to soft magnetic spinel ferrite material. In recent past due to various interesting properties, this material has attracted the interest of scientist and technologist [1-3]. Mn-Zn ferrites have high magnetic permeability, saturation magnetization, electrical resistivity, Curie temperature but low power loss and relatively low hysteresis loss [4-6]. These properties make these materials useful in electronics, computer memory chips, magnetic recording heads, microwave devices, transducers and as transformer cores materials [7-9]. Besides this MZF at nanoscale, are also used in magnetically guided drug delivery system, medical resonance imaging (MRI) and in magnetic ferrofluid technology [10]. To keep pace with rapidly developing technology, because of high permeability and low hysteresis loss, these materials can also be used to develop miniaturized size light weight electronic equipments [11].

Application of ferrite materials depend upon their physical and chemical properties. The magnetic and electric properties of these materials are effectively influenced by their chemical formulation, substituents and additives. Doping is reported to be an effective method to enhance material physical properties.

MZF have spinel structure which contains 64 tetrahedral sites (A-site) and 32 octahedral sites (B-site) in each unit cell. Out of these, 8 A-site and 16 B-site were occupied by metal cations, leading to 72 vacancies in the unit cell. Thus, Spinel crystal structure allows the substitution of different metallic and Rare Earth (RE) ions, into the lattice. Thus, doping with RE, Co^{2+}, Cu^{2+}, Mo^{6+}, Ti^{4+}, Al^{3+} and Sn^{4+} ions can alter their microstructure with significant change in electric and magnetic properties [12-18]. The changed properties are more enhanced in comparison to undoped ferrite materials.

RE ions were found to enhance physical and chemical properties of ferrites to make them suitable for industrial applications [19-21]. Swati *et al* [22] have studied the effect of increase in Gd^{3+} concentration on structural and magnetic properties of Cobalt Ferrites and reported the results related to crystallite size, lattice parameter, saturation magnetization, coercivity and remanence magnetization. Since, Gd^{3+} doped Cobalt ferrites show high resistance and low loss are suitable to be used in radio and microwave frequency applications. A. B. Kadam *et al* [23] have reported the effect of Gd^{3+} on cobalt ferrite with decrease in crystallite size, lattice parameter and saturation magnetization. V. More *et al* [24] have reported increase in lattice parameter and crystallite size with an increase in Ce^{3+}concentration in Ni-Mn-Zn ferrite. R. H. Kadam *et al* [25] have synthesized Dy^{3+} substituted Co-Cu-Zn nano ferrites by sol-gel technique and reported an increase in crystallite size, saturation magnetization, coercivity and dielectric constant with an increase in Dy^{3+} doping. M. V. Chaudhari *et al* [26] have reported decrease in crystallite size and magnetization with increase in Cr doping in $Co_{0.5}Mg_{0.5}Cr_xFe_{2-x}O_4$.

V. J. Angadi *et al* [27] have synthesized Sm^{3+} doped Mn-Zn ferrites using combustion reaction method and reported a decrease in saturation magnetization and remanence. Iqbal *et al* [28] have reported decrease in complex dielectric constant and tangent loss with an increase in Eu^{3+}ions in Mn-Zn ferrites. A. B Mugutkar *et al* [29] have reported decrease in particle size and saturation magnetization

of Co-Zn nanocrystalline ferrites with increase in Gd doping. R. A. Pawar *et al* [30] also have reported an amplification in the magnetic properties of Co-Zn ferrite nano particles on Gd^{3+} substitution.

Thus, in spite of extensive work on Rare Earth doping in ferrites and their effect on magnetic properties and particles size is not yet fully understood. Moreover, different rare-earth ions give different results in different materials. In the present work, we reported the synthesis of Samarium doped Mn-Zn ferrites (MZF: Sm), by varying the Samarium concentration (x = 0.1, 0.2% and 0.3%), using chemical co-precipitation method. The material so obtained was annealed at some higher temperatures (200°C) and then subjected to structural, morphological, compositional, optical and magnetic characterization.

2. Experimental

2.1 Materials

Manganese chloride tetra hydrate ($MnCl_2.4H_2O$), Ferric chloride ($FeCl_3$), Zinc nitrate hexa-hydrate ($ZnNO_3.6H_2O$) and Samarium oxide (Sm_2O_3) have used as source materials for the synthesis of Mn:Zn ferrites$Mn_{1-x}Zn_xFe_2O_4$ (x=0.5). The calculated (molar concentration) amount of these materials were dissolved separately in distill water. As samarium oxide is insoluble in water, HNO_3 was added in water to make it soluble. NaOH was used to adjust the pH of the solution and to make the material precipitate. To control the size and agglomeration of the precipitate particles, a surfactant (Oleic acid) was added to this solution. All the reagents used were of analytical grade and used without any further purification.

2.2 Synthesis of ferrites

The flow chart of complete synthesis process of ferrites is shown in the Figure 1. The precipitation took place at temperature 80°C. Complete precipitation took place in 90 min. The pH of the solution was adjusted at 10.

The photomicrographs of annealed undoped and Samarium doped Mn:Zn ferrite powdered precipitate is shown in Figure 2. It is clear from these photomicrographs that all samples are dark brown in color. The prepared samples were captioned as P, A, B, and C. Sample 'P' for undoped Mn-Zn Ferrites (MZF), whereas A, B and C samples referred to Sm^{3+} doped samples having concentration 0.1%, 0.2% and 0.3%, respectively.

2.3 Characterization

The powdered as-synthesized materials were annealed and then characterized using X-ray diffraction (XRD) (Rigaku Miniflex 600 make) for their structural properties. FTIR spectra were recorded with IR spectrometer, (Perkin Elmer make) to explore the presence of various functional groups. SEM studies were done for morphological characterization using Scanning Electron Microscope (ZEISS ULTRA PLUS make). TEM studies were performed on Transmission Electron Microscope (JEOL JEM 1230 120KV make). The magnetic characterization was done using VSM (Lake Shore Cryotronics 7400-S make). All these characterizations were done at room temperature.

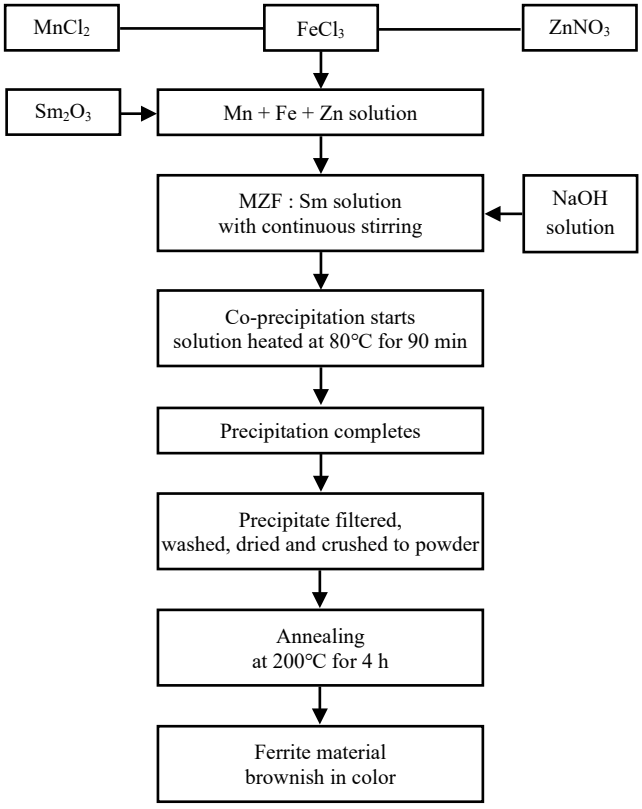

Figure 1. Flow chart of the synthesis of Ferrite materials.

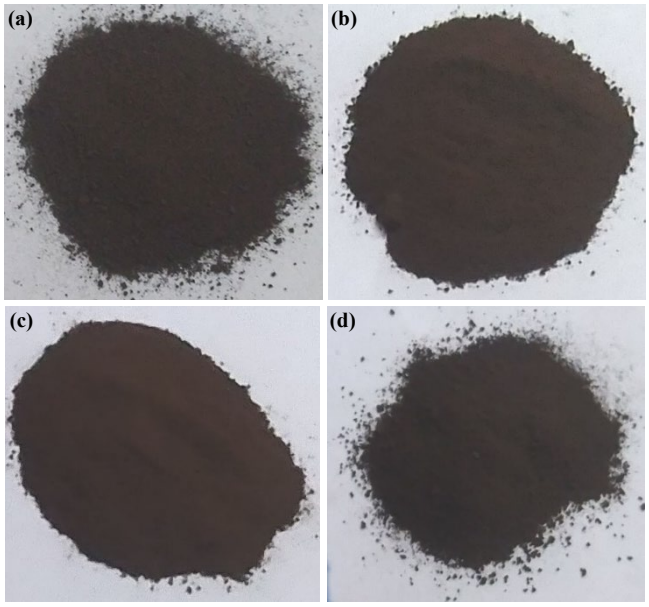

Figure 2. Powdered Samples of (a) undoped (b) 0.1 Sm^{3+} (c) 0.2 Sm^{3+}, and (d) 0.3 Sm^{3+} concentration.

3. Results and discussion

3.1 Structural properties

X-ray diffraction (XRD), being simple and non-destructive technique, was used at room temperature to determine crystalline phases, crystallite size, lattice parameters and lattice strain present

in all the samples. The XRD spectra of all the samples were recorded 2θ over the range 20° to 80°. The spectra obtained for all the samples are shown in Figure 3. All the peaks in these XRD patterns are indexed as 220, 311, 222, 400, 511, 440, and 533 with a prominent peak (311) at around 2θ=31.65° in all the samples, an indication of cubic spinel structure in pure as well as in samarium doped material. Spinel ferrite structure was observed for pure sample (sample P). Since the doped materials also indicate similar peaks, these materials also have spinel ferrite structure. These peaks when compared with that of (JCPDS Card No. 074-2401) were found to give good agreement. The sharpness of peak shows the presence of crystalline cubic phase in the material. However, some small peaks are visible with diminished intensity related to the background and hence not considered. The lattice parameters were calculated using *d* values with corresponding (hkl) values. Particle size, lattice parameters and X-ray density, respectively, were calculated using following equations [31]. The average crystallite size was calculated using Scherrer's equation:

$$D_{XRD} = \frac{k\lambda}{\beta cos\theta} \quad (1)$$

Where D_{XRD} is the average crystallite size, k is Scherrer's constant taken to be 0.9, λ is the X-ray wavelength (λ=1.5406 Å), β is the peak width at half maximum taken for prominent peak, and θ is the Bragg's diffraction angle.

The lattice parameter α was calculated for prominent peak (311), using equation 2.

$$a = d_{hkl}\sqrt{h^2 + k^2 + l^2} \quad (2)$$

Where d_{hkl} is inter-planar separation, *"a"* is lattice parameter, and *'h', 'k', 'l'* are miller indices.

The X-ray density ρ_x is determined using the equation:

$$\rho_x = \frac{ZM}{N_A V} \quad (3)$$

Where Z is the number of atoms in a unit cell corresponds to spinel structure and is taken to be 8, N_A is Avogadro number, M is molecular weight and V is volume of the cubic unit cell: a^3.

The various parameters calculated using above equations are shown in the Table 1. It is clear from the data shown in table that on doping with 0.1% Sm^{3+}, crystallite size, lattice parameter and the lattice strain decreases where as X-ray density increases as compared to their values for undoped sample P. Moreover, further increase in (0.2% and 0.3%) Sm^{3+} doping, the lattice parameter decreases where as the crystallite size increases as compare to their values at 0.1% doping. However no change in X-ray density was found at Sm^{3+} = 0.2% but a small increase in its value is observed at Sm^{3+}=0.3%. The lattice strain, after an increase at 0.2% doping shows a decrease at 0.3% of Sm^{3+}.

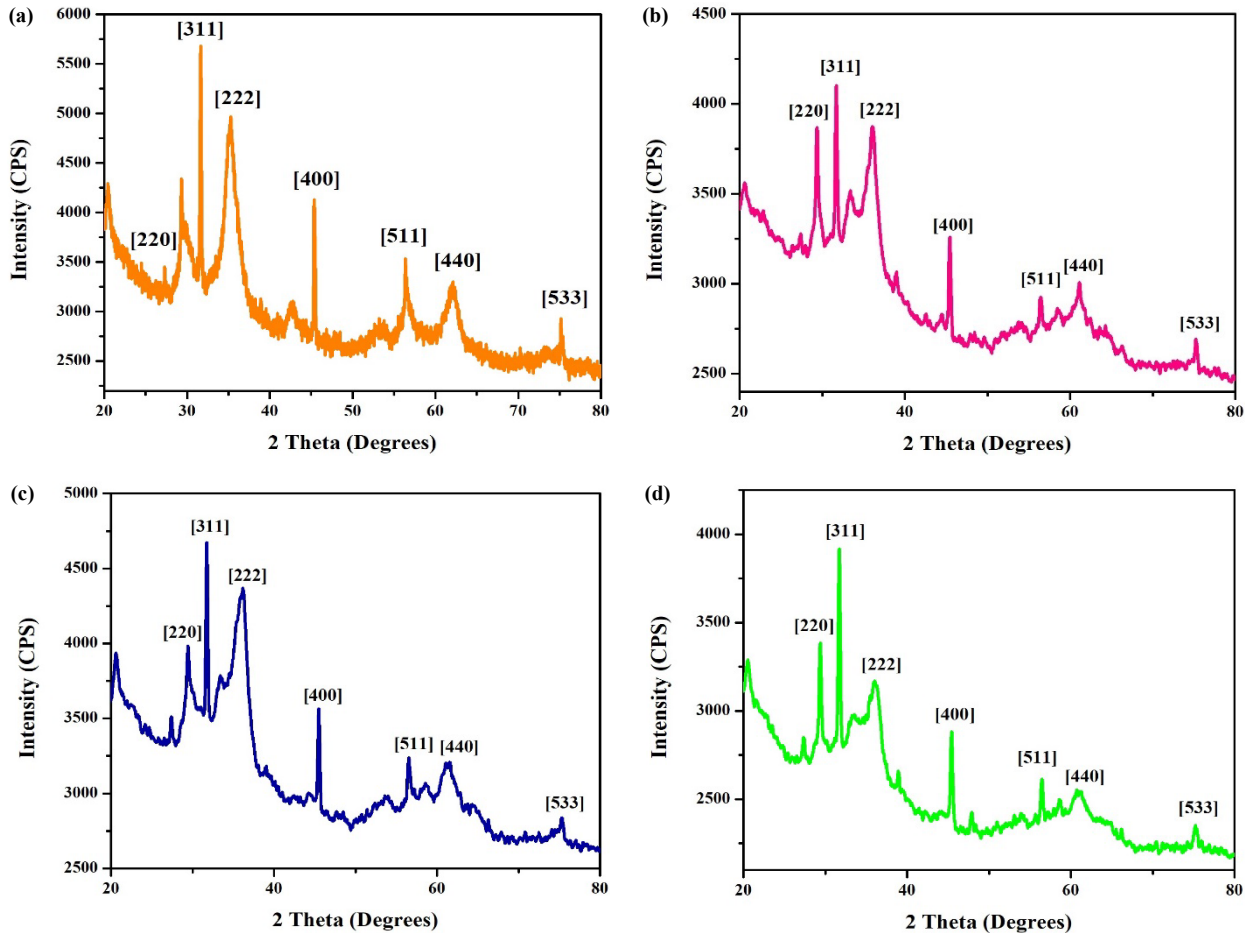

Figure 3. XRD spectra of (a) undoped and (b) 0.1%, (c) 0.2%, and (d) 0.3% Sm^{3+} doped Mn: Zn ferrites.

Table 1. Crystallite size (D), lattice Parameter (a), X-ray density (ρ), and lattice Strain (ε) for samples P, A, B and C.

Properties	Composition %			
	Undoped (Sm^{3+} = 0)	(Sm^{3+} = 0.1%)	(Sm^{3+} = 0.2%)	(Sm^{3+} = 0.3%)
Crystallite size, D (nm)	6.60	4.90	5.30	6.70
Lattice parameter, *a* (Å)	9.37	9.36	9.34	8.32
X- Ray density, ρ ($g{\cdot}cm^{-3}$)	4.70	7.20	7.20	7.30
Lattice strain, ε	1.66	1.53	1.78	1.41

The graphical variation of crystallite size and lattice parameter with Sm^{3+} concentrations are shown in Figure 4. The observed changes in crystallite size and lattice parameter on Sm^{3+} doping might be due to difference in ionic radii of parent and doping materials [32]. It is clear from Table 1, that the X-ray density for undoped sample is less than the Sm^{3+} doped samples it is because the ionic radii of Mn (0.082 nm), Zn (0.083 nm) is smaller than the ionic radii of Samarium (0.11 nm). Thus, the doping material has higher ionic radii as compared to Mn and Zn and hence higher X-ray density is expected.

3.2 Morphological studies

The morphological study of these samples was done using FESEM and TEM. The SEM micrographs of as-prepared samples obtained using Field Emission Scanning Electron Microscopy (FESEM) is shown in Figure 5. It is clear from Figure 5(a), that the surface is not smooth rather it contains very small spherical particles together with folded sheet like structure. On the whole the surface morphology is complicated having irregular shaped holes. On doping with Sm^{3+} (0.1%) concentration, the smaller particles get changed into clusters having irregular morphology (Figure 5(b)). The sheet like structure gets changed in to flower like structure with some long tunnels in between the cluster particles.

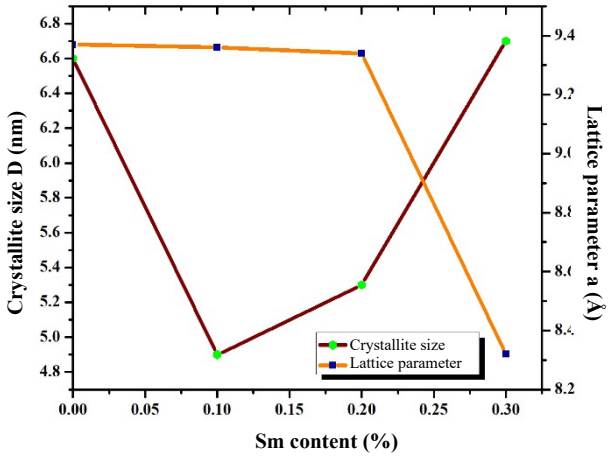

Figure 4. Variation of crystallite size and lattice parameter with Sm^{3+} ion concentrations.

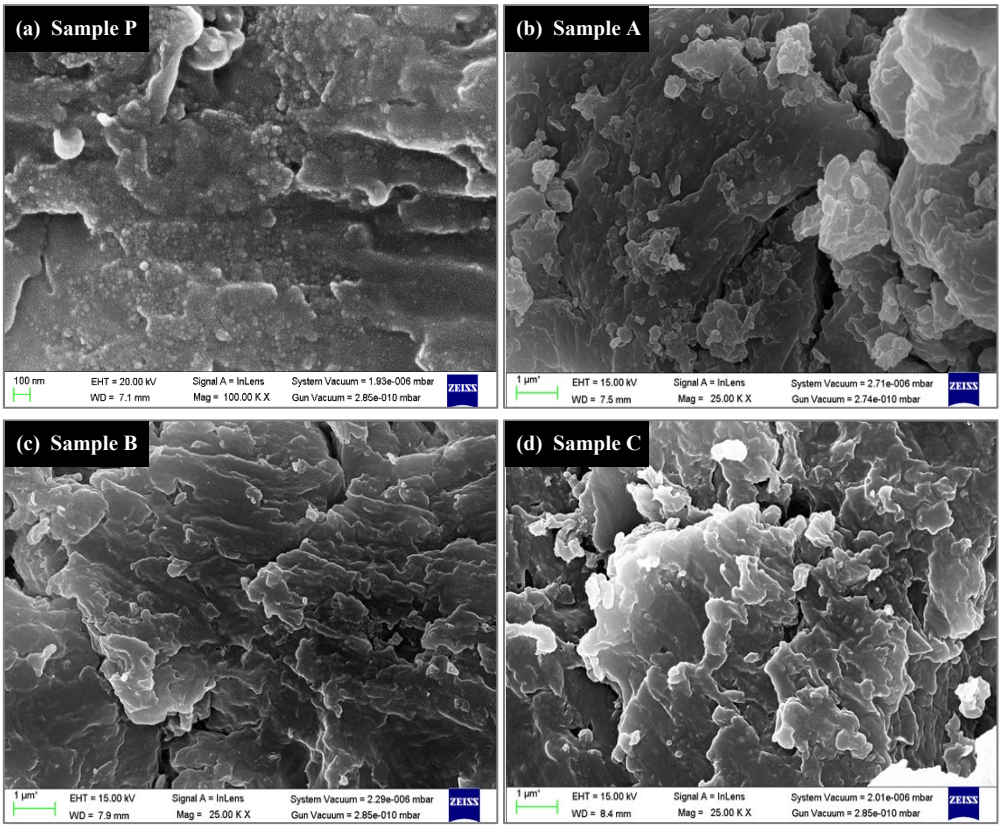

Figure 5. SEM images of undoped (a) and 0.1% (b), 0.2% (c) and 0.3%, and (d) Sm^{3+} doped Mn: Zn ferrites.

On further increase in Sm^{3+} (0.2%) concentration, the surface morphology gets further modified. Now the particle clusters are completely replaced by layer structure (Figure 5(c)). The surface has now become more smooth as compared to Figure 5(a-b). The further increase in Sm^{3+} (0.3%) concentration (Figure 5(d)), again modify the surface morphology. Now the surface indicates flower type structure with more layers and steps. Some particle clusters are further seen on the surface. The change in surface morphology on doping can be related with the change in various parameters as reported in Table 1.

Transmission Electron Microscopy (TEM) images of the as-synthesized particles are shown in the Figure 6(a-d). It is clear from Figure 6(a), that spherical particles having size (~5 nm) are non-uniformly distributed. On (0.1%) Sm^{3+} doping, (Figure 6(b)), the particle size appears to be smaller than the particle size shown in Figure 6(a), but the exact morphology is not clear. Similarly is the situation in Figure 6(c), where, the particles gets agglomerated. Thus it is clear from the results that on doping the particles size increases. These results are in good agreement with that of XRD results. Smaller size nanoparticles have higher surface area that is very beneficial for the surface related phenomena [33]. Table 2, shows the comparison between crystallite sizes calculated from XRD data and measured from TEM observations.

3.3 Composition analysis

Energy Dispersive X-Ray Analysis (EDAX) was done for compositional analysis of undoped ($Mn_{0.5}Zn_{0.5}Fe_2O_4$) and doped ($Mn_{0.5}Zn_{0.5}Sm_xFe_{2-x}O_4$) samples. EDAX spectra so obtained are shown in the Figure 7(a-d). The study confirms that all the elements, Mn, Zn, Fe, O and Sm^{3+} taken at the beginning of the synthesis are also present in the synthesized samples. The elemental composition as calculated from the spectra is summarized in the Table 3. The result shows that all the materials taken initially during the synthesis are also present after the synthesis. However their composition gets slightly changed on synthesis an indication of poor stoichiometry. EDAX results also indicate that the behavior of Sm-doping in the lattice not only affect the Fe but also Mn and Zn. Because of this the Mn content seems to be somewhat higher when the Sm-doping increased to 0.3%. It is clear from the results that though only the amount of samarium was changed (0.1 to 0.3), but this addition affects the amount of almost all other elements. This might be due to the addition of rare earth Samarium which is higher ionic radii than Mn, Zn and Fe in the host lattice..

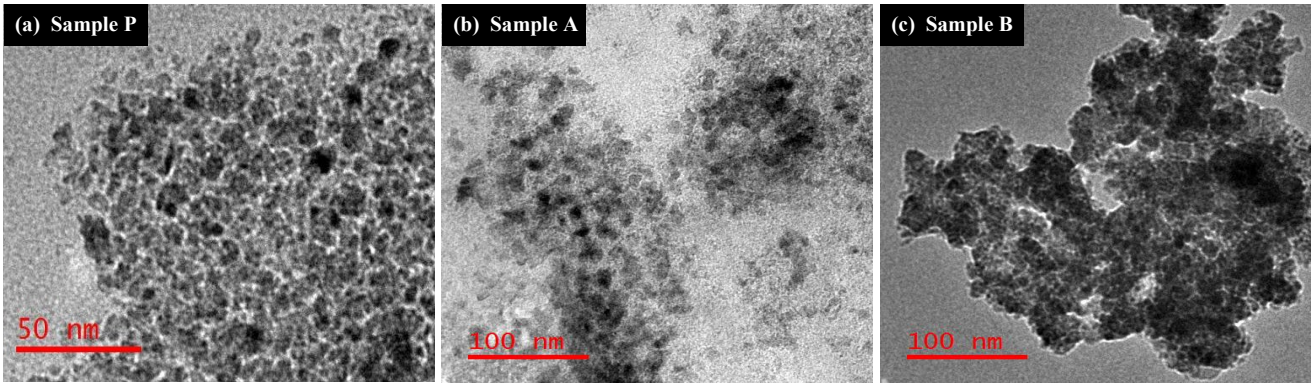

Figure 6. TEM micrograph of undoped (a) and 0.1% (b) and 0.2%, and (c) Sm^{3+} doped Mn: Zn ferrites.

Table 2. Comparative results of crystallites size calculated from XRD data and measured from TEM observations.

Samples	Crystallite size (XRD) (nm)	Crystallite size (TEM) (nm)
Sm^{3+} = 0	6.6	5.07
Sm^{3+} = 0.1%	4.9	5.2
Sm^{3+} = 0.2%	5.3	6.3
Sm^{3+} = 0.3%	6.7	-

Table 3. Compositional analysis for undoped and Sm^{3+} doped mixed Mn-Zn Ferrites.

Atomic percentage	Composition %			
	Undoped (Sm^{3+} = 0)	(Sm^{3+} = 0.1%)	(Sm^{3+} = 0.2%)	(Sm^{3+} = 0.3%)
Mn K	15.56	13.12	21.16	42.35
Zn L	17.48	19.39	22.13	13.50
Fe K	13.14	10.86	17.71	32.34
O K	53.81	56.51	38.40	9.58
Sm L	0.00	0.11	0.60	2.23

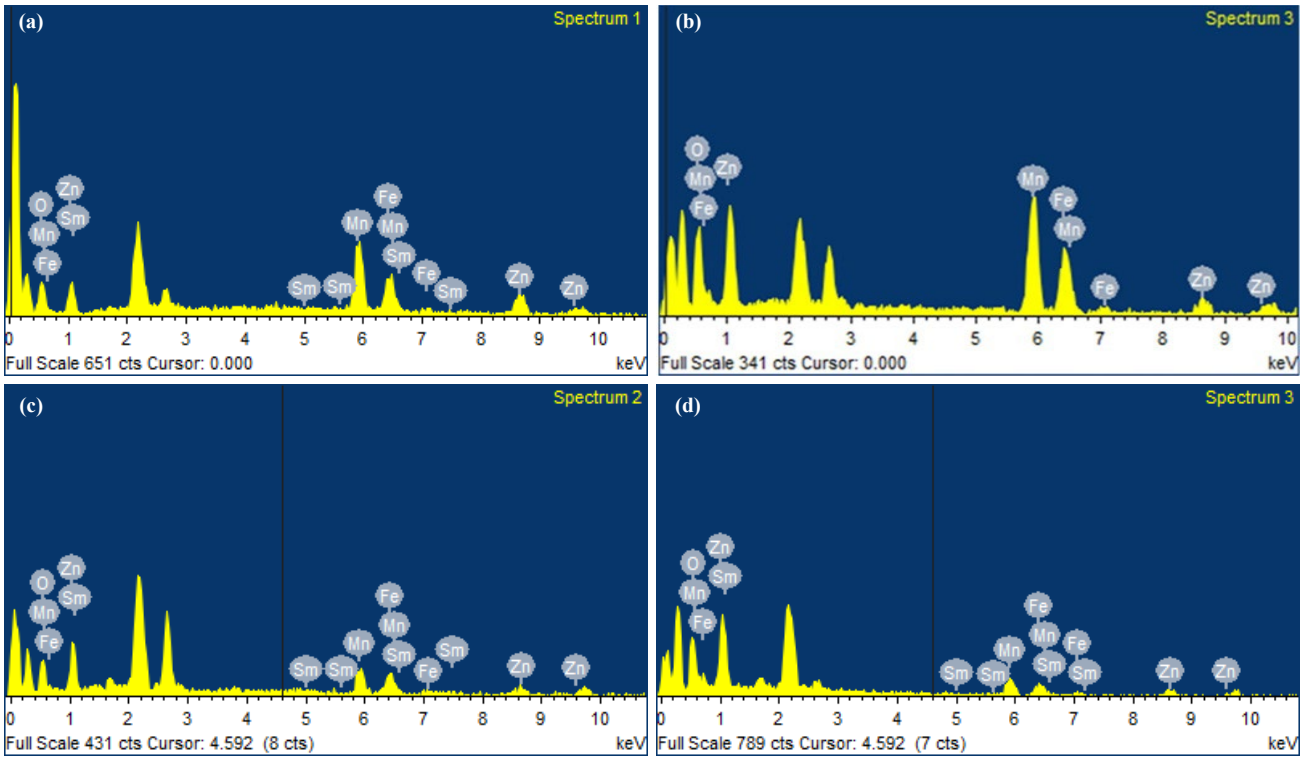

Figure 7. EDAX spectra of undoped (a) and 0.1% (b), 0.2% (c) and 0.3%, and (d) Sm^{3+} doped Mn: Zn ferrites.

3.4 FTIR analysis

The FTIR of all ferrite samples were done to identify various functional groups present in as-prepared ferrite material. The FTIR spectra were recorded over the range of 4000 cm^{-1} to 400 cm^{-1} are shown in the Figure 8(a-d). These spectra indicate various peaks at around 3450, 2925, 2850, 1740, 1595, 1378, 1220, 840, 620, 520 cm^{-1}. The peaks present in the range 700 cm^{-1} to 600 cm^{-1} are assigned due to the vibration of ferrite groups [34]. In the present work also, such peaks are observed at around 620 cm^{-1} in both, undoped and Sm^{3+} doped ferrite material. It is reported in literature that peaks present in between 500 cm^{-1} to 600 cm^{-1} are due to metal-oxygen bonding [35]. In the present observations the several peaks are present below 500 cm^{-1}in Sm^{3+} doped samples as shown in the inset of Figure 8 (b-d). Thus the rare earth ions are surrounded not only in one surroundings rather; more surroundings are present in the doped material. It is clear from Figure 8(a) that no peak is present in $Mn_{0.5}Zn_{0.5}$ Fe_2O_4 beyond 615 cm^{-1}. But on doping with Sm^{3+}additional peaks appear beyond 615 cm^{-1}. These additional peaks can be related to an outcome of Sm^{3+} doping. As shown in insets it is not single peak, rather greater number peaks are present, which are resolved only on high resolution. All these resolved peaks shift towards lower frequencies on increasing the Sm^{3+}content.This shifting is due to the substitution of Sm^{3+} cations, which have large ionic radii than that of parent material, at the octahedral site, due to which the bond lengths were increased giving rise to low vibration frequencies. A. B. Mugutkar [36] also have reported the same effect. The other peaks shown (Figure 8) in between 3450 cm^{-1} and 840 cm^{-1} are due to H-O-H, OH, C=O and C=C groups. It is clear that peak at 3424 cm^{-1} present in Figure 8(a), slowly disappears with the increasing amount of Sm^{3+}.Therefore, FTIR results confirm the incorporation of Sm^{3+} ion in the Mn-Zn Ferrites.

The addition of Sm^{3+} in Mn: Zn ferrite, affects the presence of Fe ions at tetrahedral and octahedral sites. In fact, Sm^{3+} replaces the Fe^{2+} and Fe^{3+}fromtetrahedral and octahedral sites. At tetrahedral site the Fe^{2+} is surrounded by four oxygen atoms where as at octahedral site the Fe^{3+} is surrounded by six oxygen atoms. When Fe is replaced by Sm^{3+} it also gets surrounded by four oxygen at tetrahedral site and by six oxygen at octahedral sites. Since one cannot ensure the complete replacement of Fe by Sm^{3+} and hence some Fe^{2+} and Fe^{3+} also exist at these sites. Thus Fe^{2+}-O, Fe^{3+}-O, Sm–O, Mn-O, Zn-O remain present in every doped ferrite samples. It is because of this greater numbers of peaks are present towards lower wave number i.e., around 600 cm^{-1}. Similar observation has also been reported in literature [26], where the author has taken as Cr as dopant in Mn: Zn ferrite leading to a greater number of peaks corresponding to metal-oxygen bonding. The Peak position and corresponding bonding as observed in FTIR spectra are summarized in Table 4 [37].

3.5 Magnetic properties

Magnetic parameters such as Coercivity (H_c), Remanence (M_r) and Saturation Magnetization (M_s), of the as-prepared MZF: Sm having different Sm^{3+} (0.1% to 0.3%) concentration are calculated from VSM hysteresis plots, shown in Figure 9(a-d). These results are summarized in Table 5.

It is clear from the plots drawn magnetization vs. magnetic field that the magnetization increases (49.18 emu·g^{-1}) with the increase in magnetic field but the saturation region has not yet reached. It may reach to saturation value if the corresponding magnetic field is increased to a value needed for increasing the magnetization to its saturation. On reversing the magnetic field to zero the magnetization is also reversed, but it does not become zero at zero magnetic field.

Thus, certain amount remanence, though small (1.00 emu·g^{-1}) exists at zero field. To reduce remanence zero, the magnetic field (180.12 Gauss) has to be reversed in negative direction. The magnetizing field is continued to increase in negative direction leading the magnetization to increase, but in opposite direction attaining its maximum value but not saturation. On further reducing the magnetic field to zero the magnetization is still left at zero field. Thus, this remanence is of opposite sign then the earlier one. On further increasing the magnetic field in positive direction the magnetization also increases to its maximum but not to saturation level. In this way the hysteresis loop (shown in inset) is obtained, off course having small area, an indication of small remanence. On doping with 0.1% of Sm^{3+} the similar variation of magnetization vs. magnetic field is obtained but with smaller magnetization (18.67), remanence (0.16 emu·g^{-1}) and coercivity (29.54 Gauss). On further increasing the Sm^{3+} concentration to 0.2%, the similar variation of magnetization vs. magnetic field but with increase in magnetization (28.56), reduced remanence (0.14 emu·g^{-1}) but slight increased coercivity (38.55 Gauss). Further increase in Sm^{3+} concentration to 0.3%, similar variation of magnetization vs. magnetic field is observed but with magnetization (16.76), slight increase in remanence (0.22 emu·g^{-1}) and reduced coercivity (37.76 Gauss). All these results are summarized in Table 5.

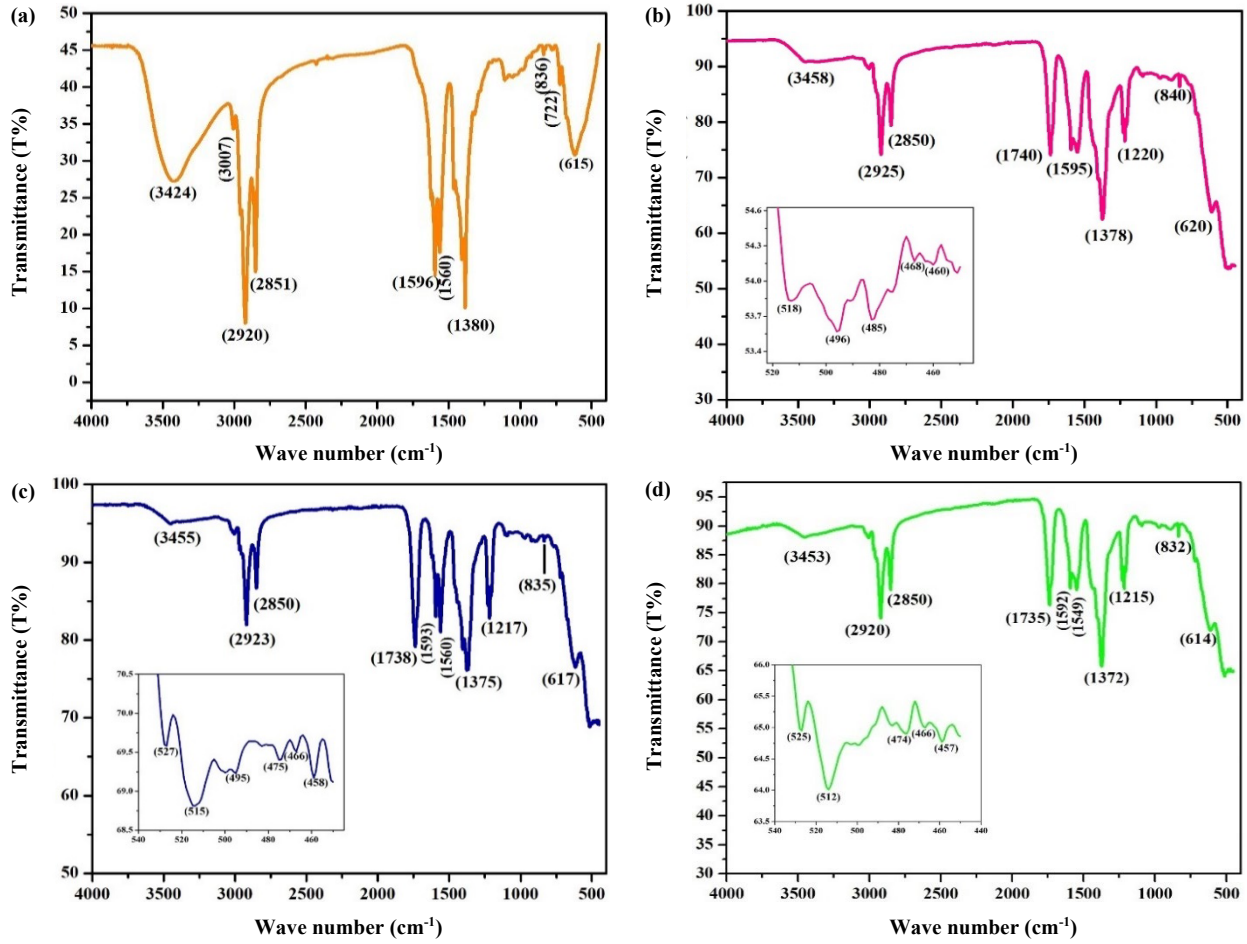

Figure 8. FTIR spectra for undoped (a), 0.1% (b), 0.2% (c), and 0.3% (d) Sm^{3+} doped Mn: Zn ferrites.

Table 4. Comparative position of FTIR Peaks in undoped and Sm- doped samples.

Standard wave number	Our observation				Bonding
(cm^{-1})	Undoped	Sm^{3+} = 0.1%	Sm^{3+} = 0.2%	Sm^{3+} = 0.3%	
3400	3424	3458	3455	3453	O-H vibrations
2900 - 2800	2922, 2852	2925, 2850	2923, 2850	2920, 2850	C – H stretching
1750 - 1725		1740	1738	1735	C = O stretching
1600 - 1550	1595, 1562	1595	1593, 1560	1592, 1549	C = C Stretching
1380 - 1200	1384	1378, 1220	1375, 1217	1372, 1215	H –O – H bending vibrations / OH deformation vibration
800 - 600	830, 719, 616	840, 620	835, 617	614	Vibration of Ferrite groups
600 - 400		518, 496, 485, 468, 460	527, 515, 495, 475, 466, 458	525,512,474, 466,457	Metal- oxygen (M – O) Stretching Vibrations

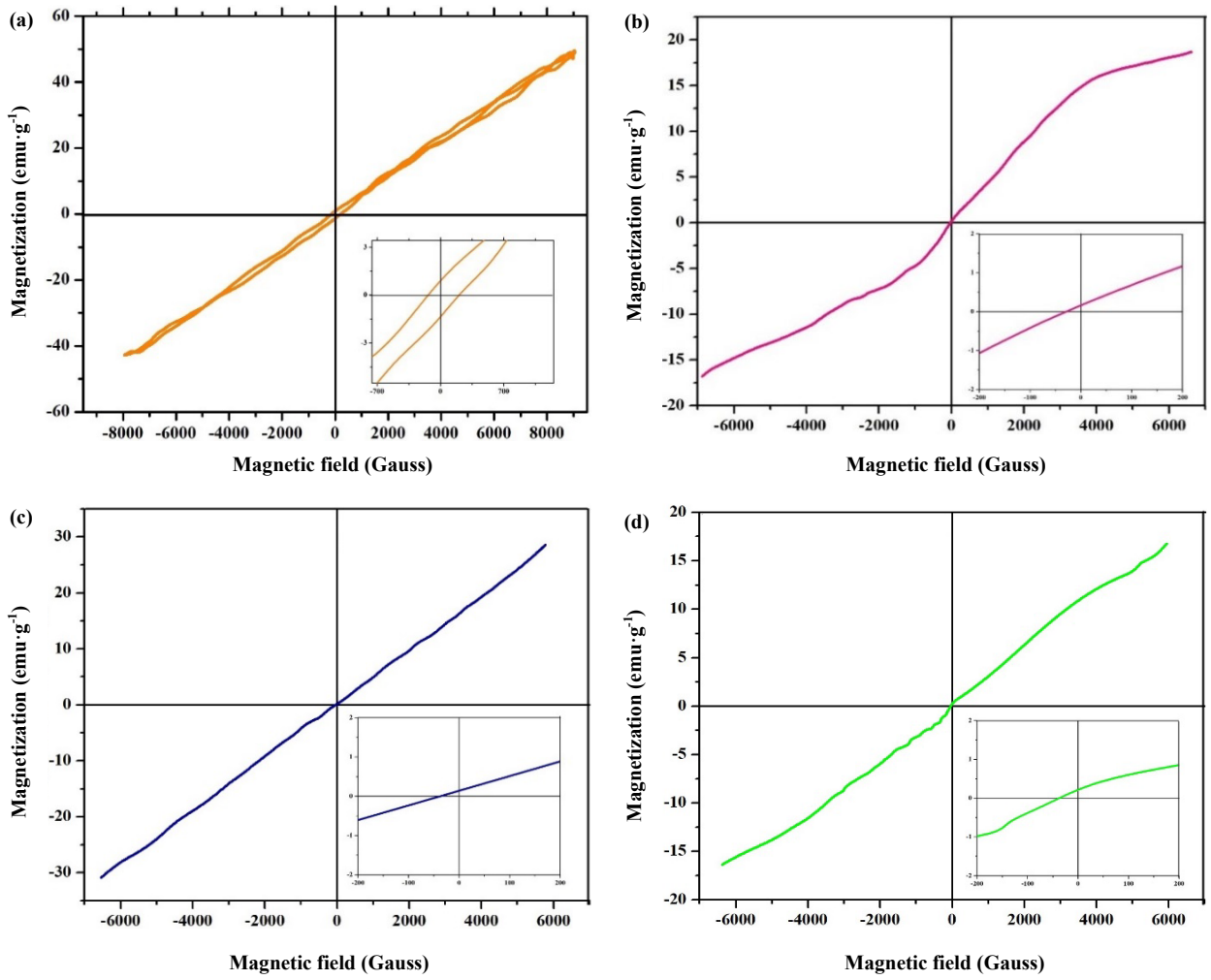

Figure 9. VSM spectra of undoped (a), 0.1% (b), 0.2% (c), 0.3% (d) Sm^{3+}doped Mn: Zn ferrites.

Table 5. Magnetic measurements of Sm^{3+} doped ferrite samples.

Properties	Composition %			
	Undoped (Sm^{3+} = 0)	(Sm^{3+} = 0.1%)	(Sm^{3+} = 0.2%)	(Sm^{3+} = 0.3%)
Saturation magnetization, M_s(emu·g^{-1})	49.18	18.67	28.56	16.76
Coercivity, H_c (gauss)	180.12	29.54	38.55	37.76
Remanence, M_r (emu·g^{-1})	1.00	0.16	0.14	0.22

All the parameters shown in the Table 5 show that, although Pure Mn: Zn ferrite show maximum magnetization. Probably for Mn:Zn ferrites, the magnetic field require for raising the magnetization to saturation magnetization is more than considered in the present study. Furthermore, the remanence is small but the coercivity is large for the pure Mixed Mn:Zn ferrites. This is the characteristic of hard ferrite which is expected as the solid solution of Mn and Zn give rise a material harder than their pure counterpart. Doping with 0.1% Sm^{3+} drops down all the three parameters *viz.* magnetization, remanence and coercivity by a considerable amount. This is expected as due to the difference in ionic radii of Sm^{3+} and that of Mn and Zn, the incorporation of Sm^{3+} in Mn: Zn lattice may distort the lattice of $Mn_{0.5}$ $Zn_{0.5}$ Fe_2O_4 ferrite. Since the incorporation of Sm^{3+}effects the distribution of Fe ions. These Fe-ions occupy either tetrahedral site or octahedral sites as Ferrous and ferric ions. The doped Sm^{3+} ion replaces Fe from both the sites and thus make the lattice strained [28]. Such changes in the distribution of Fe^{+2}, Fe^{+3} and Sm^{3+} ions in the lattice might be the reason for the observed change in magnetic parameters. Further addition (0.2%) of Sm^{3+}not only affect the lattice but also contribute to the magnetism leading to increase in magnetization and coercivity but a slight decrease in remanence. At 0.3% Sm^{3+} doping the, magnetic parameters do change but these changes are not as significant as was observed at 0.1% Sm^{3+} doping. This might be due to the fact that the ionic radii mismatch in between Sm^{3+}, Fe^{+2} and Fe^{+3}ions, the incorporation of Sm^{3+} ions at tetrahedral and octahedral site beyond certain concentration gets difficult [39]. Thus, these results confirm that the doping does affect the magnetic properties of $Mn_{0.5}Zn_{0.5}Fe_2O_4$ ferrites but only at lower doping concentration the changes are significant. Once the change has accomplished, any further increase in doping concentration do not result any significant change in magnetic parameters.

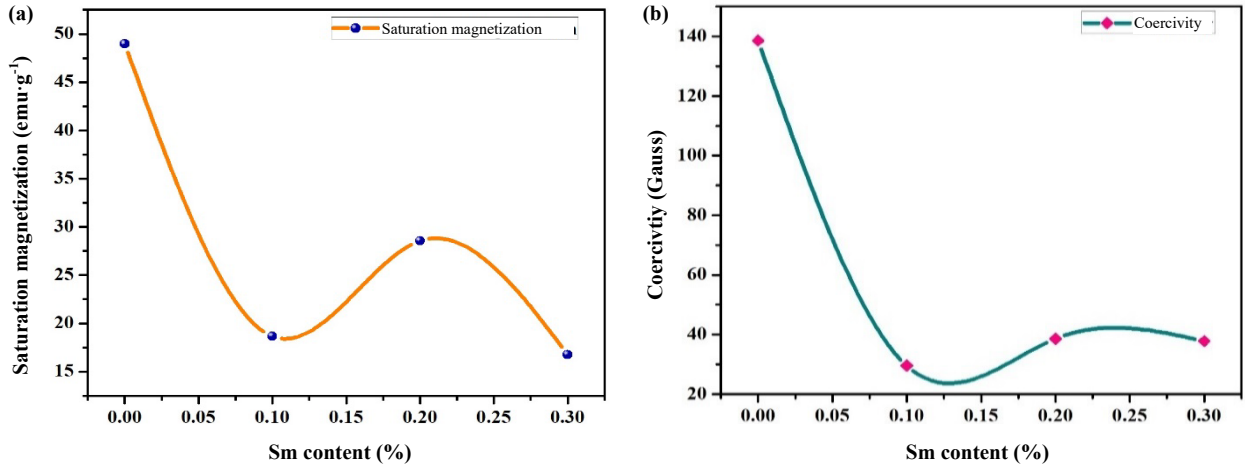

Figure 10. Variation of (a) saturation magnetization, and (b) coercivity with Sm^{3+} content.

The variations of the magnetization and coercivity with the change in Sm^{3+} content is shown in Figure 10(a-b). It is clear from these Figures that at 0.1% Sm^{3+} doping, M_s and H_c decreases sharply in comparison to their values of undoped materials. At 0.2% Sm^{3+} doping, both these parameters show significant increase in comparison to their values at 0.1% doping but remains less than the values of their undoped counterpart. However, at 0.3%, doping no significant changes in these parameters is noticed.

The continuous decrease in magnetization with an increase in Sm^{3+}doping is an indication that the material is heading towards paramagnetic rather than ferrimagnetic. Thus, it is evident from these results that Sm^{3+}doping markedly affect the magnetic properties of the Mn: Zn ferrites. The low coercive field value of Sm^{3+} doped Mn: Zn ferrites make them suitable for high frequency applications as core materials [40-42].

4. Conclusions

Undoped Manganese-Zinc Ferrite and Samarium doped (MZF:Sm) ferrites particles were successfully synthesized using chemical co-precipitation method. The Samarium concentration was varied from 0.1% to 0.3%. The precipitate material so obtained was crushed to powdered material and subjected to structural, morphological, optical and magnetic characterization. Smaller crystallites were found at 0.1% and 0.2% Sm^{3+} doping. Further increase in Sm^{3+} doping viz., 0.3%, results an increase in particle size to an extent that is comparable to that of undoped material. The TEM images also reveal non-uniform distribution of nano sized particles which do not alter even when the doping was increased to 0.2%. At higher Sm^{3+}doping the spherical morphology is clearly seen with bigger particle size. The FTIR spectra confirm the presence of all basic functional groups along with the rare earth element. The peak related to Sm^{3+} is not single; rather a group of peaks are observed which are resolved at high resolution. The magnetic parameters were also found to get changed on doping. However, these changes are significant only up to 0.2% of doping. The effect of change can easily be realized in their structure, morphology and also in magnetic properties. The magnetic parameters indicate that as-produced materials which are soft ferrimagnetic heads to paramagnetic on doping. Thus, significant changes in the properties of as-prepared materials are observed at small doping concentrations viz., (0.1% and 0.2%). Beyond these amount of doping changes are there but they are not significant. Thus the present work provides the amount of Rare Earth ions, which can significantly affect the properties of the host materials. Thus Sm^{3+}doped materials are suitable in high frequency applications.

Acknowledgement

The author acknowledges the facilities provided by IIT Roorkee for magnetic and morphological characterization and our own university for TEM studies of the synthesized materials.

Conflicts of interest

The authors declare that there exist no conflicts of interest.

References

[1] M. Sugimoto, "The past, present and future of ferrites," *Journal of American Chemical Society*, vol. 82, pp. 269-280, 1999.

[2] A. H. Lu, E. L. Salabas, and F. Schth, "Magnetic nanoparticles: Synthesis, protection, fictionalization, and application," *Angewandte Chemie International Edition*, vol. 46, no. 8, pp. 1222-1244, 2007.

[3] D. Stoppels, "Developments in soft magnetic power ferrites", *Journal of Magnetism and Magnetic Materials*, vol.160, pp. 323-328, 1996.

[4] P. Hu, H. B. Yang, D. A. Pan, H. Wang, J. J. Tian, S. G. Zhang, X. F. Wang, and A. A. Volinsky," Heat treatment effects on microstructure and magnetic properties of Mn–Zn ferrite powders," *Journal of Magnetism and Magnetic Materials*, vol. 322, pp.173-177, 2010.

[5] U. Ghazanfar, S. A. Siddiqi, and G. Abbas, "Structural analysis of the Mn–Zn ferrites using XRD technique," *Material Science and Engineering B*, vol. 118, pp.84-86, 2005.

[6] G. Ott, J. Wrba, and R. Lucke, "Recent Developments of Mn-Zn Ferrites for high permeability applications," *Journal of Magnetism and Magnetic Materials*, vol. 254-255, pp. 535-537, 2003.

[7] H. Waqus, and A. H. Quresghi, "Influence of pH on nano sized Mn–Zn ferrite synthesized by sol–gel auto combustion process," *Journal of Thermal Analysis and Calorimetry*, vol. 98, no. 2, pp. 355-360, 2009.

[8] A. D. P. Rao, B. Ramesh, P. R. M. Rao, and S. B. Raju, "X-ray diffraction studies of Sn/Nb substituted Mn-Zn ferrites," *IL Nuovo Cimento D*, vol. 20, no. 2, p. 9, 1998.

[9] H. N. Ji, Z. W. Lan, Z. Yu, Y. J. Zhi, and Z. Liu, *IEEE Applied Superior Electronic Devices*, pp. 25, 2009.

[10] V. Sepelak, P. Heitjans, and K. D. Becker, "Nanoscale spinel ferrites prepared by mechano-chemical route," *Journal of Thermal Analysis and Calorimetry*, vol. 90, no. 1, pp. 93-97, 2007.

[11] K. Q. Jiang, K. K. Li, C. H. Peng, and Y. Zhu, "Effect of multi-additives on the microstructure and magnetic properties of high permeability Mn-Zn ferrite," *Journal of Alloys and Compounds*, vol. 541, pp. 472-476, 2012.

[12] H. Anwar, and A. Maqsood "Comparison of structural and electrical properties of Co^{2+} doped Mn-Zn soft nano ferrites prepared via co-precipitation and hydrothermal methods," *Material Research Bulletin*, vol. 49, pp. 426-433, 2014.

[13] H. Bayrakdar, O. Yalçın, S. Vural, and K. Esmer, "Effect of different doping on the structural, morphological and magnetic properties for Cu doped nanoscale spinel type ferrites," *Journal of Magnetism and Magnetic Materials*, vol. 343, pp. 86-91, 2013.

[14] M. Gu, and G. Q. Liu. "Effects of MoO_3 and TiO_2 additions on the magnetic properties of manganese-zinc power ferrites," *Journal of Alloys and Compounds*, vol. 475, pp. 356-360, 2009.

[15] M. A. Gabal, A. M. Abdel-Daiem, Y. M. Al Angari, and I. M. Ismail, "Influence of Al-substitution on structural, electrical and magnetic properties of Mn-Zn ferrites nanopowders prepared via the sol-gel auto-combustion method," *Polyhedron*, vol. 57, pp. 105-111, 2013.

[16] H. N. Ji, Z. W. Lan, Z. Yu, K. Sun, and L. Z. Li, "Influence of Sn-substitution on temperature dependence and magnetic dis-accommodation of manganese-zinc ferrites," *Journal of Magnetism and Magnetic Materials*, vol. 321, no. 14, pp. 2121-2124, 2009.

[17] J. Bifa, T. Changan, Z. Quanzheng, J. Dongdong, Y. Jie, X. Jinsong, and S. Jingyu, "Magnetic properties of samarium and gadolinium co-doping Mn-Zn ferrites obtained by sol-gel auto-combustion method," *Journal of Rare Earths*, vol. 34, no. 10, pp. 1017-1023, 2016.

[18] A. B. Mugutkara, S. K. Gore, U. B. Tumberphale, V. K. V. Jadhav, R. S. Mane, S. M. Patange, S. E. Shirsath, and S. S. Jadhav, "Role of composition and grain size in controlling the structure sensitive magnetic properties of Sm^{3+} substituted nanocrystalline Co-Zn ferrites," *Journal of Rare Earths*, vol. 38, no. 10, pp. 1069-1075, 2020.

[19] Q. K. Xing, Z. J. Peng, C. B. Wang, and X. L. Fu, "Doping effect of Y^{3+} ions on the microstructural and electromagnetic properties of Mn-Zn ferrites," *Physica B: Condensed Matter*, vol. 407, no. 3, pp. 388-392, 2012.

[20] N. Lwin, M. N. A. Fauzi, S. Sreekantan, and R. Othman, "Physical and electromagnetic properties of nanosized Gd substituted Mg-Mn ferrites by solution combustion method," *Physica B: Condensed Matter*, vol. 461, no. 15, pp. 134-139, 2015.

[21] S. E. Jacobo, S. Duhalde, and H. R. Bertorello, "Rare earth influence on the structural and magnetic properties of Ni-Zn ferrites," *Journal of Magnetism and Magnetic Materials*, vol. 272-276, pp. 2253-2254, 2004.

[22] S. Tapdiya, S. Singh, S. Kulshrestha, and A. K. Shrivastava, "Micro structural analysis and magnetic characteristics of rare earth substituted cobalt Ferrite," *AIP Conference Proceedings*, vol. 1953, p. 120025, 2018.

[23] A. B. Kadam, V. K. Mande, S. B. Kadam, R. H. Kadam, S. E. Shirsath, and R. B. Borade, "Influence of gadolinium (Gd^{3+}) ion substitution on structural, magnetic and electrical properties of cobalt ferrites," *Journal of Alloys and Compounds*, vol. 840, p.155669, 2020.

[24] V. More, R. B. Borade, K. Desai, V. K. Barote, S. S. Kadam, V. S. Shinde, D. R. Kulkarn, R. H. Kadam, and S. T. Alone "Site occupancy, surface morphology and mechanical properties of Ce^{3+} Added Ni–Mn–Zn Ferrite Nano crystals Synthesized Via Sol–Gel Route" *NANO: Brief Reports and Reviews*, vol. 16, no. 5, p. 2150059, 2021.

[25] R. H. Kadam, R. B. Borade, M. L. Mane, D. R. Mane, K. M. Batoo, and S. E. Shirsath, "Structural, mechanical, dielectric properties and magnetic interactions in Dy^{3+}-substituted Co–Cu–Zn nanoferrites," *RSC Advances*, vol. 10, no. 47, p. 27911, 2020.

[26] M. V. Chaudhari, S. E. Shirsath, A. B. Kadam, R. H. Kadam, S. B. Shelke, and D. R. Mane, "Site occupancies of Co–Mg–Cr–Fe ions and their impact on the properties of $Co_{0.5}Mg_{0.5}Cr_xFe_{2-x}O_4$," *Journal of Alloy and Compounds,* vol. 552, no. 5, pp. 443-450, 2013.

[27] V. J. Angadi, B. Rudraswamy, E. Melagiriyappa, Y. Shivaraj, and S. Matteppanavar, "Effect of Sm^{3+} substitution on structural and magnetic investigation of nano sized Mn–Sm–Zn ferrites," *Indian Journal of Physics*, vol. 90, no. 8, pp. 881-885, 2016.

[28] M. A. Iqbal, M. Islamn, I. Ali, H. M. Khan, G. Mustafa, and I. Ali, "Study of electrical transport properties of Eu3+ substituted Mn-Zn-ferrites synthesized by co-precipitation technique," *Ceramics International*, vol. 39, pp. 1539-1545, 2013.

[29] A. B. Mugutkar, S. K. Gore, R. S. Mane, K. M. Batoo, S. F. Adil, and S. S. Jadhav, "Magneto-structural behaviour of Gd doped nanocrystalline Co-Zn ferrites governed by domain wall movement and spin rotations," *Ceremic International*, 2018.

[30] R. A. Pawar, S. M. Patange, A. R. Shitre, S. K. Gore, S. S. Jadhav, and S. E. Shirsath, "Crystal chemistry and single-phase synthesis of Gd3+ substituted Co–Zn ferrite nanoparticles forenhanced magnetic properties," *RSC Advances*., vol 8, p. 25258, 2018.

[31] A. Shrivastava, and A. K. Shrivastava, "Improvement in properties of Mn-Zn ferrite nanoparticles by rare earth doping," *Journal of Nano and Electronic physic*s, vol. 13, no. 2, p. 02002, 2021.

[32] R. P. Pant, M. Arora, B. Kaur, V. Kumar, and A. Kumar, "Finite size effect on Gd3+ doped CoGdxFe2-xO4 ($0.0 \leq x \leq 0.5$)

particles," *Journal of Magnetism and Magnetic Materials*, vol. 322, no. 22, pp. 3688-3691, 2010.

[33] W. Lueangchaichaweng, B. Singh, D. Mandelli, W. A. Carvalho, S. Fiorilli, and P. P. Pescarmona, "High surface area, nano-structured boehmite and alumina catalysts: Synthesis and application in the sustainable epoxidation of alkenes," *Applied Catalysis A: General*, vol. 571, pp. 180-187, 2019.

[34] U. N. Trivedi, K. H. Jani, K. B. Modi, and H. H. Joshi, "Study of cation distribution in lithium doped nickel ferrite," *Journal of Material Science Letters*, vol. 19, pp. 1271-1273, 2000.

[35] R. M. Mohamed, M. M. Rashad, F. A. Haraz, and W. Sigmund, "Structure and magnetic properties of nano-crystalline cobalt ferrite powders synthesized using organic acid precursor method," *Journal of Magnetism and Magnetic Materials*, vol. 322, no. 14, pp. 2058-2064, 2010

[36] A. B. Mugutkar, S. K. Gore, R. S. Mane, S. M. Patange, S. S. Jadhav, S. F. Shaikh, A. M. Al-Enizi, A. Nafady, B. M. Thamer, and M. Ubaidullah, "Structural modifications in Co–Zn nanoferrites by Gd substitution triggering to dielectric and gas sensing applications," *Journal of Alloys and Compounds*, vol. 844, p. 156178, 2020.

[37] J. Coates, "Interpretation of infrared spectra, a practical approach," in *Encyclopedia of Analytical Chemistry (Ed.*), p. 10815, 2000.

[38] S. Thakur, S. C. Katyal, and M. Singh, "Structural and magnetic properties of nano nickel–zinc ferrite synthesized by reverse micelle technique," *Journal of Magnetism and Magnetic Material*s, vol. 321, no. 1, pp. 1-7, 2009.

[39] L. R. Maxwell, and S. J. Pickart, "Magnetization in nickel ferrite-aluminates and nickel ferrite-Gallates," *Physical Review Journals Archive*, vol. 92, p. 1120, 1953.

[40] E. C. Snelling, "Soft ferrites: Properties and applications," *in Handbook of Modern Ferromagnetic Materials*, 2nd ed., Butterworths, London, 1969.

[41] J. Azadmanjiri, and S. A. Seyyed Ebrahimi, "Influence of stoichiometry and calcination condition on the microstructure and phase constitution of $NiFe_2O_4$ powders prepared by sol-gel autocombustion method," *Physica. Status Solidi (C)*, vol. 1, no. 12, pp. 3414-3417, 2004.

[42] B. Baruwati, R. K. Rana, and S. V. Manorama, "Further insights in the conductivity behavior of nano-crystalline $NiFe_2O_4$," *Journal of Applied Physics*, vol. 101, p. 014302, 2007.